

Regularized imaging methods for defect detection using flexural waves

Lars Hörchens (1) and Diemer de Vries (1)

(1) Laboratory of Acoustical Imaging and Sound Control, Delft University of Technology, Lorentzweg 1, 2628 CJ Delft, The Netherlands

PACS: 43.40.Dx, 43.40.Sk, 43.60.Pt

ABSTRACT

Non-destructive inspection of plates and plate-like objects is often performed by local thickness measurements requiring scanning of the object under investigation. A viable alternative is given by flexural waves, which propagate along the plate and can be used to retrieve information on remote locations by measuring the scattered field. In order to obtain an image of inhomogeneities in the plate, the dispersive characteristics of flexural waves have to be taken into account. The resolution and the quality of the resulting image can be improved by several means. The most important parameters in this context are the frequencies employed for imaging and the positions of sources and receivers with respect to the region to be imaged. On the processing side, further improvement of the quality of the obtained images can be achieved by regularizing the inverse imaging problem using a priori assumptions on the structures to be expected. Results obtained by regularization with maximal sparseness or minimal total variation are presented. As an alternative to these ‘mathematical’ regularization techniques, a more advanced physical model of the scattering can be employed to explain the measured data. Abandoning the Born approximation and including multiple scattering between the defects in the model is shown to lead to images with high resolution and low noise level.

INTRODUCTION

Plates and plate-like objects can be inspected by measuring the local material thickness using bulk waves. However, this method is time-consuming due to the required scanning of the inspected structure. The usage of guided waves forms a viable alternative: guided waves propagate along the plate. Waves being reflected or scattered from inhomogeneities in the medium can be picked up at a limited number of receiver points. In a subsequent step, the measured signals can be used to create an image showing the position and severity of defects.

In general, guided waves are dispersive: their propagation velocity depends on the frequency, such that wave fronts from an impulsive source spread out with increasing distance from the source (Auld 1973). This property has to be dealt with in order to obtain accurate information on the location of primary (excitation) or secondary (diffraction) sources in the wave field.

Flexural waves, also known as bending waves, are one member of the family of guided waves in plates. They are used in this work as a typical dispersive wave type that can easily be generated and measured. Flexural waves can be excited at relatively low frequencies and form the main cause for sound radiation from vibrating plates.

This paper is structured as follows: A method for removing the effects of dispersion from measured time signals is described, followed by a discussion of techniques for the generation of an image of material properties using information available at a limited number of receiver points. Several regularization methods for this inverse imaging problem are introduced and compared. As an alternative solution, results obtained with a more sophisticated physical model including multiple scattering are presented.

THE FLEXURAL WAVE EQUATION

The propagation of flexural waves is described by a fourth order differential equation:

$$\left(\nabla^4 - \omega^2 \frac{m}{B}\right) u(\omega, \underline{x}) = 0, \quad (1)$$

with $\underline{x} = (x, y)^T$ representing the spatial coordinate, B being the bending stiffness and m representing the mass per unit area of the plate (Cremer et al. 2005). In this simple form, the bending stiffness B is assumed to be constant, whereas the mass per unit area is allowed to vary (Leissa 1969). The Green’s function $G(\omega, \underline{x}_0, \underline{x})$ can be shown to have the following form:

$$G(\omega, \underline{x}_0, \underline{x}) = -\frac{j}{8k^2} \left[H_0^{(2)}(k\Delta x) - H_0^{(2)}(-jk\Delta x) \right], \quad (2)$$

with $\Delta x = |\underline{x} - \underline{x}_0|$, \underline{x}_0 being the point of origin, $j = \sqrt{-1}$ representing the imaginary unit and k being the wavenumber:

$$k = \sqrt{\omega} \sqrt[4]{\frac{m}{B}}. \quad (3)$$

From Eq. 3, it can be seen that the wavenumber k depends nonlinearly on the frequency ω .

For higher frequencies or higher distance from the source, the Green’s function is approximately proportional to a simple exponential function:

$$G_{\text{approx}}(\omega, \underline{x}_0, \underline{x}) \propto e^{-jk\Delta x} = e^{-j\sqrt{\omega} \sqrt[4]{\frac{m}{B}} \Delta x}. \quad (4)$$

The effects of dispersion arise due to the fact that the phase spectrum of the Green’s function depends nonlinearly on the frequency. This nonlinear dependency makes the wave fronts spread out with advancing time and with increasing distance Δx from the source.

REMOVAL OF THE EFFECTS OF DISPERSION

The dispersion relation between wavenumber and frequency described by Eq. 3 can be used to remove the effects of dispersion by performing a mapping from frequency to wavenumber in the spectral domain. In this mapping, the spectrum is resampled according to the dispersion relation. The phase spectrum depending nonlinearly on the frequency is mapped to a phase spectrum depending linearly on the wavenumber. This idea has been developed in the fields of optical communication (Brinkmeyer and Ulrich 1990) and non-destructive inspection (Wilcox 2003). Figure 1 gives an overview of the processing steps. Dispersive time signals are thereby converted to non-dispersive spatial signals providing information on the distance of an event in the wave field to the receiver point.

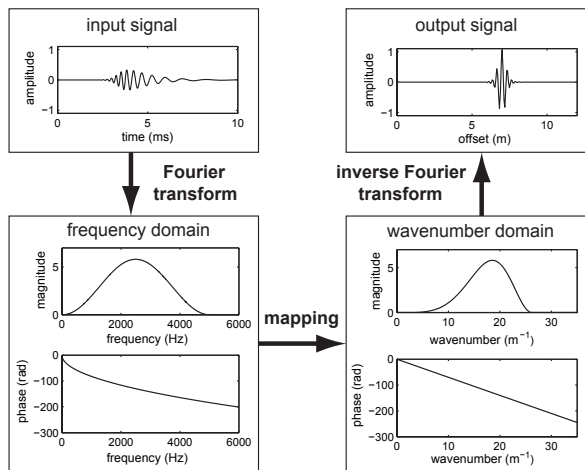


Figure 1: Schematic overview of the spectral mapping scheme for dispersion removal; a dispersive temporal signal is converted to a non-dispersive spatial signal.

This technique for dispersion compensation can be applied to a time signal measured at a single position in order to retrieve the location of a primary source, i.e., the point of excitation, or a secondary source, for instance caused by diffraction due to an inhomogeneity.

FORWARD IMAGING MODEL

A better insight in the state of the plate under investigation can be obtained by the formation of a two-dimensional image revealing the position of possible inhomogeneities. The image is generated based on measurements taken using N_s sources and N_r receivers with source index s and receiver index r for N_ω different frequencies. A single measurement is obtained by using one source-receiver pair. The incident wave field $u_{\text{inc}}(\omega, s, \underline{x})$ caused by each source is assumed to be known. The total field $u(\omega, s, \underline{x})$ that can be observed is modeled as the sum of the incident and the scattered field:

$$u(\omega, s, \underline{x}) = u_{\text{inc}}(\omega, s, \underline{x}) + u_{\text{sc}}(\omega, s, \underline{x}). \quad (5)$$

It satisfies the wave equation for the position-dependent wavenumber:

$$\left[\nabla^4 - k(\underline{x})^4 \right] u(\omega, \underline{x}) = 0, \quad (6)$$

whereas the incident field satisfies the wave equation for the wavenumber k_0 of the plate without inhomogeneities:

$$\left(\nabla^4 - k_0^4 \right) u_{\text{inc}}(\omega, \underline{x}) = 0. \quad (7)$$

Subtracting Eq. 7 from Eq. 6, the following wave equation is obtained for the scattered field caused by the inhomogeneities:

$$\left(\nabla^4 - k_0^4 \right) u_{\text{sc}}(\omega, \underline{x}) = \left[k(\underline{x})^4 - k_0^4 \right] u(\omega, \underline{x}) = k_0^4 \chi(\underline{x}) u(\omega, \underline{x}). \quad (8)$$

The scattered field can thus be interpreted as a field caused by material inhomogeneities acting as secondary sources that are activated by the total field. The source term on the right hand side of Eq. 8 is usually referred to as the *contrast sources* $w(\omega, \underline{x})$:

$$w(\omega, s, \underline{x}) = k_0^4 \chi(\underline{x}) u(\omega, s, \underline{x}). \quad (9)$$

The inhomogeneities, i.e., local deviations in material properties, are represented by a position-dependent dimensionless contrast function $\chi(\underline{x})$:

$$\chi(\underline{x}) = \frac{k(\underline{x})^4}{k_0^4} - 1. \quad (10)$$

If there is no inhomogeneity present, $k(\underline{x}) = k_0$, and the contrast is equal to zero. In order to be able to apply the simple bending wave equation given by Eq. 1, the contrast has to be dependent on a change in mass per unit area only. This means, for instance, that the model tries to explain a physically present change in material thickness by a change in mass density for reasons of simplicity. A similar choice is often made for the calculation of the scattered field of acoustic waves by assuming the mass density to be constant and explaining all observations by changes in compressibility. However, it must be noted that such a simplifying approximation might limit the performance of the imaging algorithm (van Dongen and Wright 2007).

The Born approximation

If the contrast and the total wave field are known, the scattered field is easily calculated by the spatial convolution of the Green's function for flexural waves with the contrast sources defined by Eq. 9:

$$u_{\text{sc}}(\omega, s, \underline{x}) = k_0^4 \int_{-\infty}^{\infty} G(\omega, \underline{x}, \underline{x}_0) \chi(\underline{x}_0) u(\omega, s, \underline{x}_0) d\underline{x}_0. \quad (11)$$

The operator \mathbf{G} is introduced as a short notation for this calculation:

$$u_{\text{sc}}(\omega, s, \underline{x}) = \mathbf{G}w(\omega, s, \underline{x}_0). \quad (12)$$

It can be seen that there exists an implicit relation between the total field and the scattered field: the scattered field depends on the total field, which is formed by the incident and the scattered field. The problem can be simplified by application of the Born approximation, which assumes that the total field incident on the scatterer can be approximated by the incident field (De Hoop 1995). This approximation is valid if the scattered field is much smaller than the incident field. A concurrent estimation of both the total field and the contrast is thereby avoided.

$$u_{\text{sc}}(\omega, s, \underline{x}) \approx k_0^4 \int_{-\infty}^{\infty} G(\omega, \underline{x}, \underline{x}_0) \chi(\underline{x}_0) u_{\text{inc}}(\omega, s, \underline{x}_0) d\underline{x}_0. \quad (13)$$

The scattered field measured at the receiver locations \underline{x}_r can then be calculated:

$$u_{\text{sc}}(\omega, s, r) \approx k_0^4 \int_{-\infty}^{\infty} G(\omega, \underline{x}_r, \underline{x}) \chi(\underline{x}) u_{\text{inc}}(\omega, s, \underline{x}) d\underline{x}. \quad (14)$$

This operation can be expressed by the operator \mathbf{G}_R performing a mapping from the contrast to the receiver signals for a given incident field:

$$u_{\text{sc}}(\omega, s, r) = \mathbf{G}_R \chi(\underline{x}). \quad (15)$$

THE INVERSE IMAGING PROBLEM

The reconstruction of the contrast $\chi(\underline{x})$ from measurements $u_{sc}(\omega, s, r)$ at the receiver points for possibly different source positions is known as the inverse imaging problem. In a straightforward approach, Eq. 15 can formally be inverted in a least-squares sense:

$$\chi(\underline{x}) = \left(\mathbf{G}_R^\dagger \mathbf{G}_R \right)^{-1} \mathbf{G}_R^\dagger u_{sc}(\omega, s, r), \quad (16)$$

with the superscript dagger denoting the hermitian adjoint of an operator. The operator \mathbf{G}_R is, in general, ill-conditioned, such that direct inversion is not possible. Hence, stabilization and possibly regularization are required to overcome the ill-posedness. There exist several strategies to tackle this objective, some of which are discussed in the following sections.

Backpropagation

A first approximation to the full inversion as presented in Eq. 16 is given by applying only the adjoint operator:

$$\chi(\underline{x}) = \mathbf{G}_R^\dagger u_{sc}(\omega, s, r). \quad (17)$$

This approach is known as backpropagation. From a physical point of view, it provides a correct solution only for the phase spectrum. Therefore, it enables correct localization of inhomogeneities, but provides rather poor resolution due to the fact that the amplitude spectrum is not perfectly inverted.

Furthermore, the positions of sources and receivers determine to what extent the wavenumber spectrum of the inhomogeneities can be retrieved in the image (Langenberg 2002). A coincident source-receiver pair, for instance, is able to retrieve spectral content at wavenumbers equivalent to half the wavelength of the frequency employed for imaging. This setup is thus adequate for the imaging of strong, localized transitions in material properties. A resolution of approximately half a wavelength must be regarded as the general limit for imaging under the Born approximation (Wolf 1969).

In a tomography setup with source and receiver on opposite site of the region to be imaged, spectral content corresponding to lower wavenumbers can be retrieved. Hence, such a setup is suited for the detection of gradual variations of material properties over a larger region. For optimal imaging setups, both aspects have to be combined. The ideal constellation is obtained if the imaging region is surrounded by sources and receivers.

Figure 2 shows a simulation setup for an aluminum plate of 3 mm thickness with a number of transducers able to act as both sources and receivers. The transducers are positioned on a semicircle on one side of the imaging domain.

The region to be imaged contains three inhomogeneities, the true contrast of which is depicted in Fig. 3. In the simulations, the full forward problem including multiple scattering is solved, and the total field in the plate is calculated. Four different frequencies between 500 Hz and 4 kHz are used for the imaging process. In order to make the simulations more realistic, 10 % noise is added to the receiver signals.

The imaging result obtained by backpropagation is shown in Fig. 4. The constellation of defects can be recognized. However, the defect on the left side is imaged more clearly than the one on the top. This is due to the fact that the array of sources and receivers positioned to the right of the imaging region images the vertically oriented defect as a strong reflector, whereas the horizontally oriented defect of equal severity reflects significantly less energy towards the array. It is recognizable only by the diffraction from its tips.

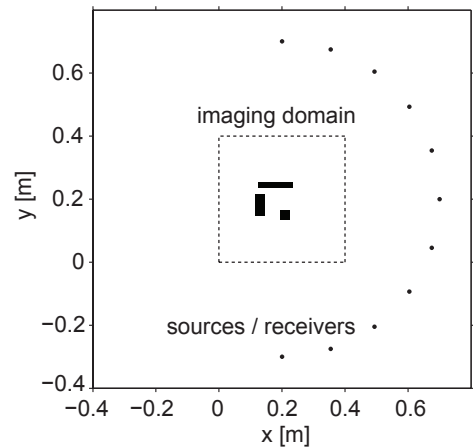


Figure 2: Simulation setup used for the calculation of the receiver signals.

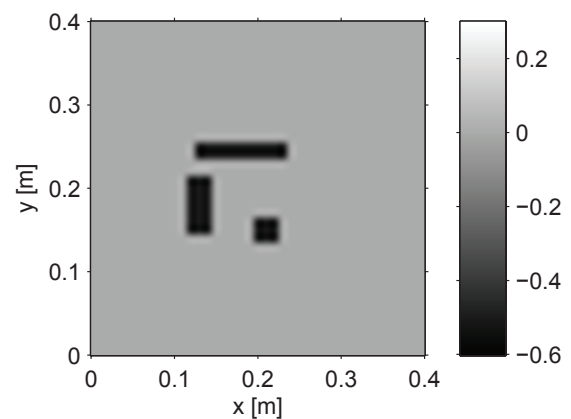


Figure 3: Image of the true contrast as used in the simulation.

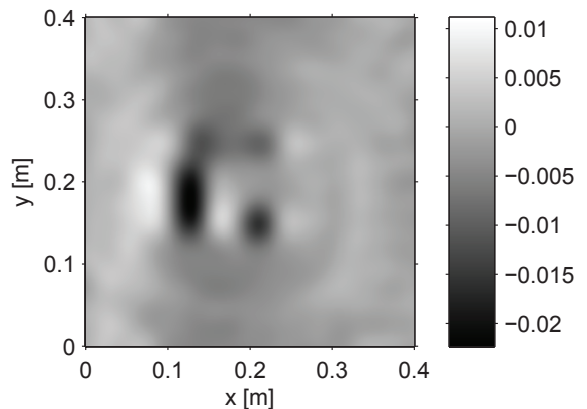


Figure 4: Imaging result obtained by backpropagation.

Regularized imaging

If the resolution cannot be optimized by choosing a different frequency range or a different setup of sources and receivers, regularization of the inverse imaging problem provides another method of increasing the resolution of the resulting image.

A common choice is the well-known Tikhonov regularization:

$$\chi(\underline{x}) = \left(\mathbf{G}_R^\dagger \mathbf{G}_R + \gamma \mathbf{I} \right)^{-1} \mathbf{G}_R^\dagger u_{sc}(\omega, s, r), \quad (18)$$

with γ being an operator controlling the strength of the regularization Hansen (1998).

Tikhonov regularization minimizes the energy of the estimated image. A common criticism of such a type of regularization is the smoothness of the results produced. The parameter γ has to be carefully chosen to find an optimum between an overly smoothed result and the unwanted amplification of measurement noise.

An image obtained by inversion with Tikhonov regularization is shown in Fig. 5. Inversion compensates for the difference in sensitivity of the array with respect to horizontally and vertically oriented defects. All three defects can be recognized. However, even with smoothing regularization, the noise present in the data is amplified and causes severe artifacts, some of which could be regarded as false positives.

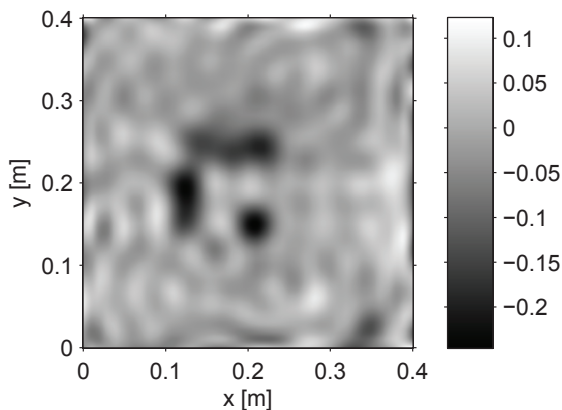


Figure 5: Imaging result obtained by inversion with Tikhonov regularization. The object can be recognized, but severe artifacts caused by measurement noise are visible as well.

Instead of using general mathematical regularization methods, a more useful image can be obtained by means of a regularizer relying on a priori knowledge on the typical structure of the image to be expected. In the following, two regularizers of this kind, namely a sparseness constraint and a total variation constraint, are presented and compared.

Sparseness constraint

The assumption of sparseness is useful if the imaging result is expected to contain only a few localized defects, whereas the biggest part of the image shows no deviation from the standard medium properties. There are different methods of promoting sparseness in an inversion scheme. In this work, the approach of Sacchi and Ulrych is adapted (Sacchi et al. 1998). The additive regularization term is chosen to be position-dependent. Stronger regularization is thereby applied to regions for which there is little information from the data:

$$\chi(\underline{x}) = \left[\mathbf{G}_R^\dagger \mathbf{G}_R + \gamma \mathbf{Q}(\underline{x}) \right]^{-1} \mathbf{G}_R^\dagger u_{sc}(\omega, s, r), \quad (19)$$

with the operator $\mathbf{Q}(\underline{x})$ having the following form:

$$\mathbf{Q}(\underline{x}) = 1 + \frac{|\chi(\underline{x})|^2}{2\sigma^2}. \quad (20)$$

This operator can be derived by assuming the amplitudes of the image values to obey a Cauchy distribution. The parameter σ is used to control the amount of sparseness. Both regularization parameters γ and σ can be chosen automatically based on the

expected sparseness (Zwartjes 2005) and the maximum amplitudes in the image (Hörchens 2010). Both the regularizing term \mathbf{Q} and the estimate of the contrast χ are then updated alternately in an iterative scheme.

Figure 6 shows the image obtained with sparse inversion. It can be seen that the noise is significantly better damped in comparison to the image generated using Tikhonov inversion as shown in Fig. 5. The point-like defect is recovered with superior resolution. The extended inhomogeneities, however, are less visible. For the defect on the top, only the two tips can be seen. The information on extended defects that is only weakly present in the measurements is suppressed for the sake of fulfilling the sparseness constraint.

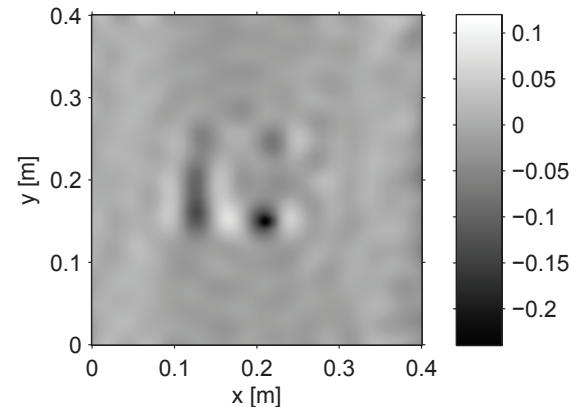


Figure 6: Imaging result obtained by inversion with sparse regularization. Point-like structures and tips of extended defects are retrieved better than regions of constant contrast.

If it is known in advance that the inhomogeneities to be detected are point-like, the sparse regularizer can help to achieve excellent resolution. However, if smooth variations in material properties or less severe defects are present, it is likely that these are suppressed in favor of point-like structures. Therefore, it is possible that defects are missed, despite the fact that there is actually evidence for their presence in the measured data.

Total variation constraint

A less presumptive method is given by minimizing the total variation of the obtained image. The regularizing functional E to be minimized is based on the magnitude of the image gradient and has the following form:

$$E = \int_{-\infty}^{\infty} |\nabla \chi(\underline{x})| d\underline{x}. \quad (21)$$

In the present work, an iterative inversion scheme presented by Abubakar et al. is applied (Abubakar et al. 2004). In this scheme, the total variation constraint is included as a multiplicative term, such that no extra regularization parameters have to be chosen. The total variation constraint allows for slow variations and sharp transitions while at the same time reducing the influence of measurement noise on the resulting image. This kind of regularization can be characterized as more appropriate for general defect detection than the sparseness constraint.

The imaging result obtained by inversion with regularization by total variation is shown in Fig. 7. The inhomogeneities can clearly be seen, and noise is suppressed to a sufficient extent. The main difference to the true contrast as depicted in Fig. 3 is the incorrect estimation of the severity of the defects as can be seen from the color scales in both figures.

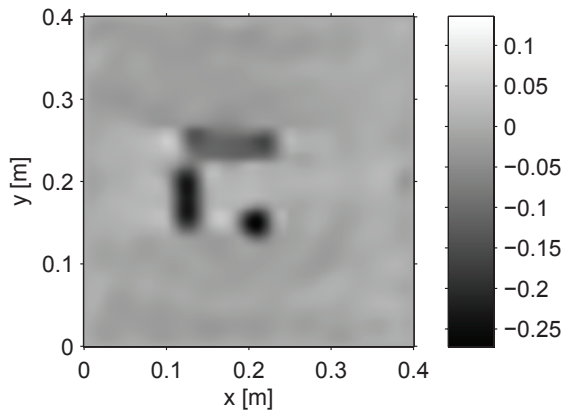


Figure 7: Imaging result obtained by inversion with minimum total variation as regularization constraint. A good balance between the suppression of noise and the retrieval of the shapes of the inhomogeneities is found.

IMAGING BEYOND THE BORN APPROXIMATION

An alternative to the inclusion of assumptions on the structure of the image to be expected is the usage of a more sophisticated physical imaging model. If the Born approximation is abandoned, multiple scattering present in the measurement data can be used for the generation of the image, thereby improving the accuracy and resolution of the result (Simonetti 2006).

Contrast source inversion

The main problem is given by the fact that the total wave field in the plate is not known in advance. Therefore, the total wave field must be estimated along with the contrast. To this end, the *contrast source inversion* (CSI) method is applied (van den Berg et al. 1999). Contrast source inversion starts out from a rough estimate of the contrast sources, the total field, and the contrast. Such an estimate can be obtained by backpropagation:

$$w_0(\omega, s, \underline{x}) = \mathbf{G}^\dagger u_{sc}(\omega, s, r), \quad (22)$$

$$u_0(\omega, s, \underline{x}) = u_{inc}(\omega, s, \underline{x}) + \mathbf{G} w_0(\omega, s, \underline{x}), \quad (23)$$

$$\chi_0(\underline{x}) = \frac{1}{N_\omega} \sum_{\omega=1}^{N_\omega} \frac{\sum_{s=1}^{N_s} w_0(\omega, s, \underline{x}) u_0^*(\omega, s, \underline{x})}{k_0^4 \sum_{s=1}^{N_s} |u_0(\omega, s, \underline{x})|^2}, \quad (24)$$

with the superscript asterisk denoting the complex conjugate. The estimate of the contrast given by Eq. 24 can be obtained by inverting the definition of the contrast sources (Eq. 9) in a least-squares sense, with the information available at different frequencies weighted equally (Hörchens 2010).

In subsequent iterations, two error functionals are minimized:

1. The receiver signals must be caused by the contrast sources:

$$E_R = \sum_{\omega=1}^{N_\omega} \frac{\|u_{sc}(\omega, s, r) - \mathbf{G}_R w(\omega, s, \underline{x})\|_R^2}{\|u_{sc}(\omega, s, r)\|_R^2}, \quad (25)$$

with $\|\cdot\|_R$ being the L^2 -norm with respect to the receiver signals.

2. The incident and the scattered field must add up to the total field:

$$E_D = \sum_{\omega=1}^{N_\omega} \frac{\|k_0^4 \chi u_{inc} - w + k_0^4 \chi \mathbf{G} w\|_D^2}{\|k_0^4 \chi u_{inc}\|_D^2}, \quad (26)$$

with $\|\cdot\|_D$ being the L^2 -norm with respect to the domain of the wave field. In this equation, the explicit dependency on variables has been dropped for the sake of a short and clear notation.

The above functionals are minimized by a conjugate gradient scheme, in which updates for the different variables are obtained in the following order:

1. First, a new estimate of the contrast sources $w(\omega, s, \underline{x})$ is calculated.
2. In a second step, the total field $u(\omega, s, \underline{x})$ is updated based on the current estimate of the contrast sources.
3. Subsequently, a new estimate of the contrast $\chi(\underline{x})$ can be obtained from the current total field and the contrast sources.

The image obtained by contrast source inversion is shown in Fig. 8. The inhomogeneities are significantly better retrieved than by inversion under the Born approximation (Fig. 5). By taking multiple scattering into account, the imaging model is able to make use of the full potential of the measured data. Under the Born approximation, the part of the wave field due multiple scattering cannot be explained by the simplified model and ends up as noise causing imaging artifacts.

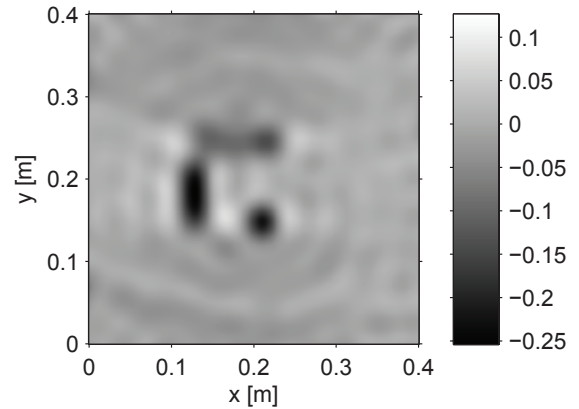


Figure 8: Imaging result obtained by contrast source inversion. The inclusion of multiple scattering has a positive effect on the obtained resolution and the suppression of noise.

It can be stated that the inclusion of multiple scattering acts as a kind of regularization. However, in contrast to methods presented above, it is not based on assumptions on the typical image structure. On the contrary, contrast source inversion uses the evidence already present in the data to achieve a better imaging result.

It is, of course, possible to combine contrast source inversion with additional regularization. Figure 9 presents the imaging result obtained by contrast source inversion with regularization by total variation. The inhomogeneities are even better retrieved than in Fig. 8.

However, even with an imaging model including multiple scattering, the severity of the defects is underestimated as can be seen by comparing the color scales of Figs. 3 and 9. The strength of the contrast is more easily reconstructed if measurements are taken all around the region of interest, and not only on a semicircle. In the case that a full circular array is used, Fig. 10 shows that the not only the shape, but also strength of the inhomogeneities is correctly retrieved.

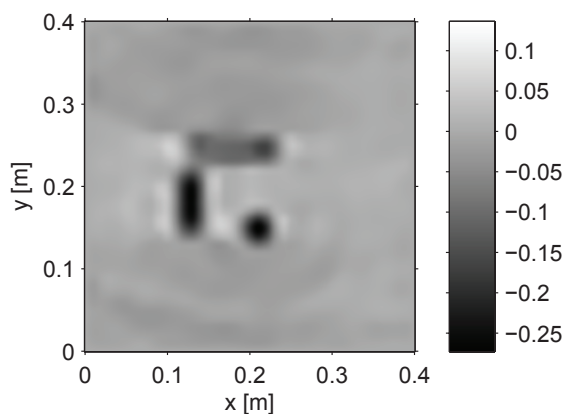


Figure 9: Imaging result obtained by contrast source inversion with additional regularization by total variation, compare to Fig. 8.

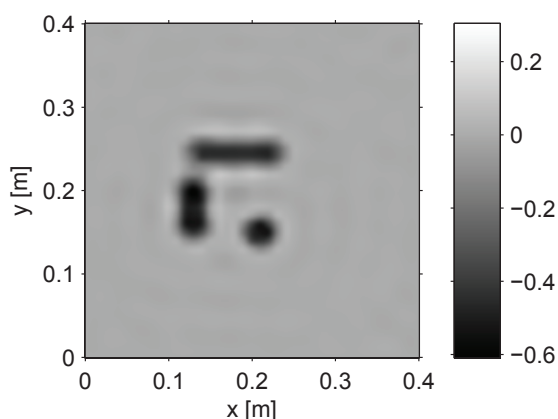


Figure 10: Imaging result obtained by contrast source inversion with additional regularization by total variation for a full circular setup of sources and receivers around the imaging domain. The quality of the image is further improved, and the strength of the contrast is retrieved correctly.

CONCLUSIONS

Several methods for imaging in flexural wave fields have been presented. As a preliminary tool, dispersion compensation can provide a first estimate of the position of primary and secondary sources. A better insight is obtained by using techniques for the generation of two-dimensional images. Based on an imaging model, several methods have been presented and compared.

As the only non-iterative method, backpropagation enables the rough assessment of the object under investigation. Better results can be achieved by inversion, which has to be regularized in order to obtain useful results. The sparse regularization constraint has been shown to be too presumptive to be applicable to defect detection in general, while minimization of the total variation has led to satisfying results.

If the Born approximation is abandoned and an imaging model including multiple scattering is used, images with high resolution and low noise level can be generated. Additional regularization can be shown to be useful, but not essential for the image quality. In order to obtain quantitatively correct estimates, a setup of sources and receivers surrounding the imaging region has to be preferred.

ACKNOWLEDGEMENTS

The authors would like to thank Peter van den Berg and Koen van Dongen for their suggestions and comments. This research is supported by the Dutch Technology Foundation STW, which is the applied science division of NWO, and the Technology Programme of the Ministry of Economic Affairs.

REFERENCES

- Aria Abubakar, Peter M. Van Den Berg, Tarek M. Habashy, and Henning Braunsch. A multiplicative regularization approach for deblurring problems. *IEEE Transactions on Image Processing*, 13(11):1524–1532, 2004.
- Bertram A. Auld. *Acoustic fields and waves in solids*. Wiley Interscience, New York, 1973.
- Ernst Brinkmeyer and Reinhard Ulrich. High-resolution OADR in dispersive waveguides. *Electronics Letters*, 26(6):413–414, 1990.
- Lothar Cremer, Manfred Heckl, and Björn A.T. Petersson. *Structure-borne sound*. Springer, Berlin, third edition, 2005.
- Adrianus T. De Hoop. *Handbook of radiation and scattering of waves*. Academic Press, London, 1995.
- Per C. Hansen. *Rank-deficient and discrete ill-posed problems: numerical aspects of linear inversion*. Society for Industrial and Applied Mathematics, Philadelphia, 1998.
- Lars Hörchens. *Imaging of material inhomogeneities with flexural waves*. PhD thesis, Delft University of Technology, 2010.
- Karl J. Langenberg. Linear scalar inverse scattering. In Roy Pike and Pierre Sabatier, editors, *Scattering and inverse scattering in pure and applied science*, pages 121–141. Academic Press, London, 2002.
- Arthur W. Leissa. *Vibration of plates*. Scientific and Technical Information Division, NASA, Washington, 1969.
- Mauricio D. Sacchi, Tadeusz J. Urych, and Colin J. Walker. Interpolation and extrapolation using a high-resolution discrete fourier transform. *IEEE Transactions on Signal Processing*, 46(1):31–38, 1998.
- Francesco Simonetti. Multiple scattering: The key to unravel the subwavelength world from the far-field pattern of a scattered wave. *Physical Review E*, 73(3, 36619), 2006.
- Peter M. van den Berg, A. L. van Broekhoven, and Aria Abubakar. Extended contrast source inversion. *Inverse Problems*, 15:1325–1344, 1999.
- Koen W. A. van Dongen and William M. D. Wright. A full vectorial contrast source inversion scheme for three-dimensional acoustic imaging of both compressibility and density profiles. *The Journal of the Acoustical Society of America*, 121(3):1538–1549, 2007.
- Paul D. Wilcox. A rapid signal processing technique to remove the effect of dispersion from guided wave signals. *IEEE Transactions on Ultrasonics, Ferroelectrics and Frequency Control*, 50(4):419–427, 2003.
- Emil Wolf. Three-dimensional structure determination of semi-transparent objects from holographic data. *Optics Communications*, 1(4):153–156, 1969.
- Paul M. Zwartjes. *Fourier reconstruction with sparse inversion*. PhD thesis, Delft University of Technology, 2005.